Hindawi
Journal of Function Spaces
Volume 2023, Article ID 2824703, 11 pages
https://doi.org/10.1155/2023/2824703

Research Article

Couple Stress Sodium Alginate-Based Casson Nanofluid Analysis through Fick's and Fourier's Laws with Inclined Microchannel

Dolat Khan,[1] **Musawa Yahya Almusawa**,[2] **Waleed Hamali**,[2] **and M. Ali Akbar**[3]

[1]*Faculty of Science, King Mongkut's University of Technology Thonburi (KMUTT), 126 Pracha Uthit Rd., Bang Mod, Thung Khru, Bangkok 10140, Thailand*
[2]*Department of Mathematics, Faculty of Science, Jazan University, Saudi Arabia*
[3]*Department of Applied Mathematics, University of Rajshahi, Bangladesh*

Correspondence should be addressed to M. Ali Akbar; ali.akbar@ru.ac.bd

Received 22 October 2022; Revised 3 December 2022; Accepted 24 March 2023; Published 19 April 2023

Academic Editor: Yusuf Gurefe

Casson nanofluid plays a vital role in food industries with sodium alginate nanoparticles. That is why many researchers used Casson nanofluid in their study. Due to this, the main objective of this study is to investigate the inclined microchannel flow of a Casson nanofluid based on sodium alginate (SA) under a few stresses. Because the plate at $y = d$ is stationary and the plate at $y = 0$ is in motion, the fluid flows. Physically existent things utilize partial differential equations as a method of derivation. By using dimensionless variables, the underlying PDEs are dimensionless. Applying Fourier's and Fick's laws to the time-fractional model makes the classical model dimensionally stable by generalization. A generalized fractional model is solved using the Laplace and Fourier integral transformations. In addition, the parametric influence of other physical elements, such as the Casson parameter, coupling velocity, temperature, and stress parameters, is considered (Grashof, Schmidt, and Prandtl numbers). Concentration distributions are shown using graphs and discussed with accompanying text. We compute and describe the Sherwood number, rate of heat transfer, and skin friction. It is concluded that skin friction and Nusselt number can be enhanced by adding nanoparticle. Also, the fractional derivative makes the study more realistic by incorporating Fick's and Fourier's laws as compared to the classical one.

1. Introduction

The term "nanomaterials" means materials that have a size of 100 nanometers or less, while nanotechnology refers to the kind of technology that produces these materials. The structure of nanomaterials as well as their characteristics is taken into consideration when classifying them into one of four groups [1]. Choi [2] was the first researcher to investigate the terminology associated with nanofluids. He came up with the term "nanofluid" to describe the fluids that included particles with diameters of less than 100 nanometers. Karthik et al. explained the rationale behind why nanosized particles are favored over microsized particles in a variety of applications [3]. Significant improvements in thermophysical characteristics have been seen when comparing nanoparticles to microparticles. Nanofluids may be used for a variety of purposes, including the cooling of air conditioning systems, the cooling of power plants, and the improvement of diesel generator efficiency [4]. Normally, water and ethylene glycol are used as the basis fluids in heat transfer systems. The manufacturing of nanoparticles involves the use of a variety of components, which may be generally classified as metallic, such as copper [5], metal oxide, such as iron oxide, and carbon-based, such as graphite. CuO [6], chalcogenide sulfides, selenides, and tellurides, all of which were discussed [7], along with several other particles, such as carbon nanotubes [8]. According to the available research, the average size of a single particle ranges from

20 to 100 nm [9, 10]. A type of nanofluid flow in a porous media with Newtonian heating and magnetohydrodynamic flow of Casson-type fluid is studied by Khan et al. [11].

In 1959, Casson came out with the first Casson fluid model. Oka [12] was the first person to look at fluids from Casson in tubes. Honey, blood, soup, jelly, stuff, slurries, and artificial fluids are all types of Casson fluids. Ahmad et al. [13] wrote about Casson nanofluid that was heated in a Newtonian way. Khan et al. [14] investigated the effects of a magnetic field, a chemical reaction, heat generation, and Newton cooling law, on the flow of Casson fluid over a moving stretched surface in a porous medium. Furthermore, Mackolil and Mahanthesh [15] examined the exact and statistical analysis of Casson nanofluid. Statistical techniques like probable error and regression are used to examine the rate of heat transfer and skin friction. Besides, many studies are reported to investigate the statistical analysis for various nanofluids [16–18]. Recently, Satya Narayana et al. [19] report a 3D flow for Casson-type couple stress nanofluid. It is discovered that the non-Newtonian pair stress fluid's temperature is greater than that of the viscous case. For increased heat transmission, it may be proposed that the matching viscous fluid in industrial applications be switched out for the Casson couple stress nanofluid.

Couple stress fluids (CSF) are different from standard viscous fluids in that they have a specific material constant. These fluids' (CSFs) rheological characteristics have a wide range of applications such as the crude oil extraction process, the solidification of liquid crystals, electrostatic precipitations, aerodynamic heating phenomena, and colloidal and suspension solutions [20]. Stokes [21] developed the idea of CSF theory, where he incorporated CSFs into account in addition to the classical Cauchy stress. It is the most straightforward modification of the theory of the conventional fluid that takes into account polar effects like the presence of CSs and body couples. Stokes provides a thorough explanation of CSF theory in his work *Theories of Fluids with Microstructure* [22], where he also lists a variety of issues that scholars have examined in relation to couple stress theory. The phenomena of pumping fluids, the synthesis of lubricants and biological processes, the solidification of liquid crystals, and the solidification of animal blood are only a few illustrations of the extraordinary applications of CSF models in our everyday life. Researchers have taken the CSF model into consideration for a variety of scientific and physical problems. Many fascinating problems involving CSFs or micropolar fluids may be found in the references [23, 24]. Khan et al. [25] used the time-fractional derivative definitions of Caputo-Fabrizio to find the solutions to the two phase CS fluid channel flow. Ali et al. [26] have looked at the flow of laminar and unstable pair stress fluid between infinite numbers of plates. Using lubricant as the base fluid, Laplace and Fourier transforms were used to find exact solutions. They found that adding nanoparticles to engine oil made the oil 12.8% more effective.

Fractional calculus [27] is the study of the many ways that differentiation and integration can be used to find the power of real and complex numbers. Ross [28] explained how fractional calculus changed from 1695 to 1900. Many physical and natural problems cannot be shown by the classical derivative, so fractional calculus is used to solve these problems. Scientists have been very interested in fractional derivatives for the past 30 years. In response to this interest, many scientists have come up with different ways to explain what a fractional derivative is. Riemann-Liouville [29] was the most typical approach to describing things in the 18th century. Despite the fact that the R-L formulation of the fractional derivative has been shown to perform effectively in many physical contexts, there are two basic approaches to applying this concept. Differentiating the constant term may not result in zero, and certain aspects of the Laplace transform are irrelevant in practice. Caputo fractional derivatives are utilized in physics, chemistry, economics, and other fields of research. They may also be employed in everyday situations. CFD is used to investigate processes such as diffusion, signal processing, material mechanical characteristics, image processing, pharmacokinetics, damping, and bioengineering. CFD [30] is a modified version of fractional calculus that corrects the issues produced by the R-L formulation. However, since the CFD kernel contains a singularity, CFD cannot be utilized to represent certain materials with large differences [31]. It cannot give a good description of what happened. Caputo-Fabrizio [32] suggests a new definition with a kernel that is not singular to get around the singularity problem in CFD. Several researchers [33–37] looked at this new idea as part of their work. CF fractional derivative is used by a number of studies to look at the effect on memory. Akhtar [38] used time-fractional Caputo and CF derivatives to study the flow of couple stress fluids (CSFs) between two parallel plates.

The existing literature does not take into consideration the fact that by utilizing Fick's and Fourier's laws, closed-form solutions for the flow of Casson fluid down a microchannel may be discovered. In terms of pair stress, we focused on the plate's motion at $y = 0$, which generates a flow SA-based Casson nanofluid through an inclined microchannel. The governing partial differential equations are nondimensionalized by employing dimensionless variables, and the energy and mass equations are fractionalized using Fick's and Fourier's laws. Caputo's definition is applied to the fractional model, and the resulting partial differential equations (PDEs) are solved by combining Laplace and Fourier transforms. Tables and figures are used to graphically present the data. It is possible to calculate the effect of various parameters on the skin friction, Nusselt number, and Sherwood number.

2. Mathematical Formulation

Consider the flow of CS SA-based Casson nanofluid along with the inclined microchannel. The flow is considered in the x-direction. Initially $(t \leq 0)$, both the fluid and the plates are at rest with the same concentration C_d and temperature T_d. After some time $(t > 0)$, the plate at $y = 0$ is carried with constant velocity $u_0 H(t)$, where u_0 is the characteristic velocity, while the second plate stays static. The moving plate's temperature and concentration rise to T_1 and C_1,

respectively, and then remain constant, as illustrated in Figure 1.

The continuity and momentum equation of the CSNF and energy equation are given by

$$\begin{aligned}
&\nabla \cdot \vec{V} = 0,\\
&\rho_{\mathrm{nf}} \frac{\partial \vec{V}}{\partial t} = -\nabla p - \mu_{\mathrm{nf}} \nabla \times \nabla \times \vec{V} - \lambda \nabla \times \nabla \times \nabla \times \nabla \times \vec{V}\\
&\qquad + g(\rho\beta_T)_{\mathrm{nf}}(T - T_\infty) + \rho_{\mathrm{nf}} \vec{b}_1,\\
&(\rho Cp)_{\mathrm{nf}} \frac{\partial \vec{T}}{\partial t} = k_{\mathrm{nf}} \nabla \times \nabla \times \vec{T},\\
&D_{\mathrm{nf}} \frac{\partial \vec{C}}{\partial t} = k_{\mathrm{nf}} \nabla \times \nabla \times \vec{C}.
\end{aligned} \tag{1}$$

Since unidirectional flow has been taken into consideration, the provided flow's velocity, temperature, and concentration fields are as follows:

$$\left.\begin{aligned}
&\vec{V} = (u(\zeta, t), 0, 0),\\
&\vec{T} = (T(\zeta, t), 0, 0),\\
&\vec{C} = (C(\zeta, t), 0, 0).
\end{aligned}\right\} \tag{2}$$

Equation for an incompressible Casson fluid flow

$$\begin{aligned}
&\tau = \tau_0 + \mu_{\mathrm{nf}} \dot{\gamma},\\
&\tau = \begin{cases} 2\left(\mu_n + \dfrac{P_\lambda}{\sqrt{2\pi}}\right) e_{ab}, \pi > \pi_c,\\ 2\left(\mu_n + \dfrac{P_\lambda}{\sqrt{2\pi_c}}\right) e_{ab}, \pi < \pi_c. \end{cases}
\end{aligned} \tag{3}$$

Under these, we get the final problem formulation as follows:

$$\begin{aligned}
\rho_{\mathrm{nf}} \frac{\partial u(\zeta, t)}{\partial t} &= \mu_{\mathrm{nf}} \left(1 + \frac{1}{\beta}\right) \frac{\partial^2 u(\zeta, t)}{\partial \zeta^2} - \lambda \frac{\partial^4 u(\zeta, t)}{\partial \zeta^4}\\
&\quad + (\rho\beta_T)_{\mathrm{nf}} g \cos(\gamma)(T - T_d)\\
&\quad + (\rho\beta_C)_{\mathrm{nf}} g \cos(\gamma)(C - C_d),
\end{aligned} \tag{4}$$

$$\frac{\partial T(\zeta, t)}{\partial t} = -\frac{1}{(\rho C_P)_{\mathrm{nf}}} \frac{\partial q(\zeta, t)}{\partial \zeta}. \tag{5}$$

Fourier's law:

$$\frac{1}{k_{\mathrm{nf}}} q(\zeta, t) = -\frac{\partial T(\zeta, t)}{\partial \zeta}. \tag{6}$$

The thermal balance equation:

$$\frac{\partial C(\zeta, t)}{\partial t} = -\frac{\partial S(\zeta, t)}{\partial \zeta}. \tag{7}$$

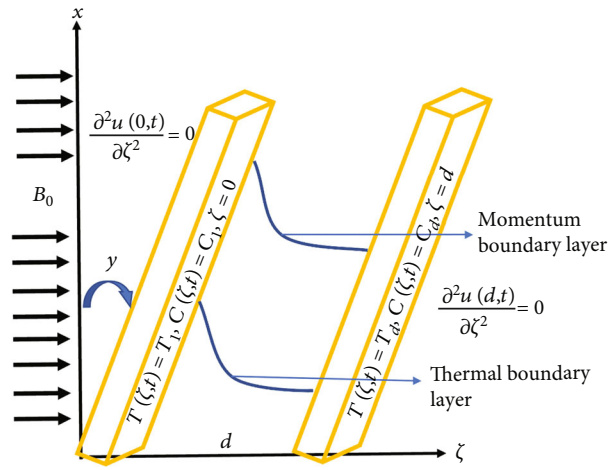

FIGURE 1: Geometry of the flow.

Fick's law:

$$\frac{1}{D_{\mathrm{nf}}} S(\zeta, t) = -\frac{\partial C(\zeta, t)}{\partial \zeta}. \tag{8}$$

These are the physical conditions:

$$\left.\begin{aligned}
&u(\zeta, t)|_{t-0} = 0, u(\zeta, t)|_{\zeta=0} = u_0 H(t), u(\zeta, t)|_{\zeta=d} = 0,\\
&T(\zeta, t) = T_d, C(\zeta, t) = C_d, t = 0,\\
&T(\zeta, t) = T_1, C(\zeta, t) = C_1, \zeta = 0,\\
&T(\zeta, t) = T_d, C(\zeta, t) = C_d, \zeta = d,\\
&\frac{\partial^2 u(0, t)}{\partial \zeta^2} = \frac{\partial^2 u(d, t)}{\partial \zeta^2} = 0.
\end{aligned}\right\} \tag{9}$$

Terms for $(\rho C_p)_{\mathrm{nf}}, (\rho\beta_T)_{\mathrm{nf}}, (\rho\beta_C)_{\mathrm{nf}}, \mu_{\mathrm{nf}}, \rho_{\mathrm{nf}}, D_{\mathrm{nf}}, k_{\mathrm{nf}}$ are given by Khan et al. [11].

$$\begin{aligned}
\mu_{\mathrm{nf}} &= \mu_f \frac{1}{(1 - \phi)^{2.5}},\\
\rho_{\mathrm{nf}} &= \rho_f(1 - \phi) + \rho_s \phi,\\
\rho_{\mathrm{nf}} &= \rho_f(1 - \phi) + \rho_s \phi,\\
(\rho C_p)_{\mathrm{nf}} &= (\rho C_p)_f(1 - \phi) + (\rho C_p)_s \phi,\\
(\rho\beta_T)_{\mathrm{nf}} &= (\rho\beta_T)_f(1 - \phi) + (\rho\beta_T)_s \phi,\\
(\rho\beta_C)_{\mathrm{nf}} &= (\rho\beta_C)_f(1 - \phi) + (\rho\beta_C)_s \phi,\\
D_{\mathrm{nf}} &= D_f \frac{1}{1 + \phi}.
\end{aligned} \tag{10}$$

To get a PDE system without dimensions, we define the following variables without dimensions:

$$\begin{aligned} u^* &= \frac{u}{u_0}, \\ \zeta^* &= \frac{\zeta}{d}, \\ T^* &= \frac{T - T_d}{T_1 - T_d}, \\ t^* &= \frac{vt}{d^2}, \\ C^* &= \frac{C - C_d}{C_1 - C_d}, \\ q^* &= \frac{qd}{k_f(T_1 - T_d)}, \\ S^* &= \frac{Sd}{k_f(C_1 - C_d)}. \end{aligned} \tag{11}$$

By eliminating the $*$ signs and replacing them with these dimensionless variables, Equations (4)–(9) become

$$\begin{aligned} \frac{\partial u(\zeta,t)}{\partial t} = \frac{b_2}{b_1}\beta_1 \frac{\partial^2 u(\zeta,t)}{\partial \zeta^2} - \frac{1}{b_1}\lambda \frac{\partial^4 u(\zeta,t)}{\partial \zeta^4} \\ + \frac{b_3}{b_1} T(\zeta,t)\mathrm{Gr}\cos(\gamma) \\ + \frac{b_4}{b_1} C(\zeta,t)\mathrm{Gm}\cos(\gamma), \end{aligned} \tag{12}$$

$$\frac{\partial T(\zeta,t)}{\partial t} = -\frac{b_6}{\mathrm{Pr} b_5}\frac{\partial q(\zeta,t)}{\partial \zeta}, \tag{13}$$

$$q(\zeta,t) = -\frac{\partial T(\zeta,t)}{\partial \zeta}, \tag{14}$$

$$\mathrm{Sc}\frac{\partial C(\zeta,t)}{\partial t} = -\frac{1}{b_7}\frac{\partial S(\zeta,t)}{\partial \zeta}, \tag{15}$$

$$S(\zeta,t) = -\frac{\partial C(\zeta,t)}{\partial \zeta}, \tag{16}$$

$$\left.\begin{aligned} &u(\zeta,t)|_{t-0} = 0, u(\zeta,t)|_{y=0} = 1, u(d,t)|_{\zeta=d} = 0, \\ &T(\zeta,t) = T_d, C(\zeta,t) = 0, t = 0, \\ &T(\zeta,t) = 1, C(\zeta,t) = 1, \zeta = 0, \\ &T(\zeta,t) = 0, C(\zeta,t) = 0, \zeta = d, \\ &\frac{\partial^2 u(0,t)}{\partial \zeta^2} = \frac{\partial^2 u(d,t)}{\partial \zeta^2} = 0, \end{aligned}\right\} \tag{17}$$

$$\begin{aligned} b_1 &= 1 - \phi + \phi\frac{\rho_s}{\rho_f}, \\ b_2 &= \frac{1}{(1-\phi)^{2.5}}, \\ b_3 &= 1 - \phi + \phi\frac{(\rho\beta_T)_s}{(\rho\beta_T)_f}, \\ b_4 &= 1 - \phi + \phi\frac{(\rho\beta_C)_s}{(\rho\beta_C)_f}, \\ b_5 &= 1 - \phi + \phi\frac{(\rho C_p)_s}{(\rho C_p)_f}, \\ b_6 &= \frac{k_s + 2k_f - 2\phi(k_f - k_s)}{k_s + 2k_f + \phi(k_f - k_s)}, \\ b_7 &= \frac{1}{1+\phi}, \\ \beta_1 &= 1 + \frac{1}{\beta}. \end{aligned} \tag{18}$$

The general FAFL are used in the following ways:

$$q(\zeta,t) = -{}^C D_t^{1-\alpha}\left(\frac{\partial T(\zeta,t)}{\partial \zeta}\right), \quad 0 < \alpha \le 1, \tag{19}$$

$$S(\zeta,t) = -{}^C D_t^{1-\alpha}\left(\frac{\partial C(\zeta,t)}{\partial \zeta}\right), \quad 0 < \alpha \le 1. \tag{20}$$

In this equation, ${}^C D_t^{1-\alpha}(.)$ stands for the Caputo time-fractional operator, and its definition is as follows:

$${}^C D_t^{\alpha}(K_1(\zeta,t)) = \frac{1}{\Gamma(1-\alpha)}\int_0^t (t-s)^{-\alpha} K_1(\zeta,t)ds = K(\zeta,t) * \xi_\alpha(t). \tag{21}$$

In this case, $\xi_\alpha(t) = t^{-\alpha}/\Gamma(1-\alpha)$ is the singular power law kernel. Moreover,

$$\begin{aligned} L(\xi_\alpha(t)) &= \frac{1}{s^{(1-\alpha)}}, \\ (\xi_{1-\alpha}(t) * \xi_\alpha(t)) &= 1, \\ \xi_0(t) &= L^{-1}\left(\frac{1}{s}\right) = 1, \\ \xi_1(t) &= L^{-1}(1) = \delta(t). \end{aligned} \tag{22}$$

In this instance, $\delta(t)$ is for a Dirac delta function. It is possible to write using Equation (21) and the properties mentioned in (22):

$$\left.\begin{aligned} {}^C D_t^0(K_1(\zeta,t)) &= K_1(\zeta,t) - K_1(\zeta,0), \\ {}^C D_t^1(K_1(\zeta,t)) &= \frac{\partial C(\zeta,t)}{\partial t}. \end{aligned}\right\} \tag{23}$$

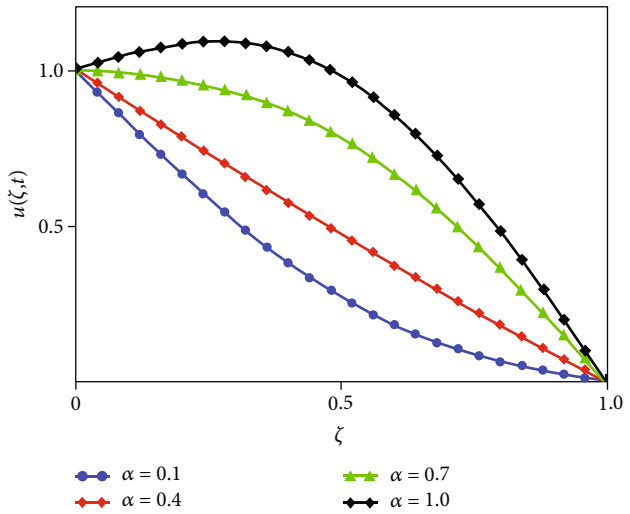

Figure 2: Influence of several values of α on velocity profile.

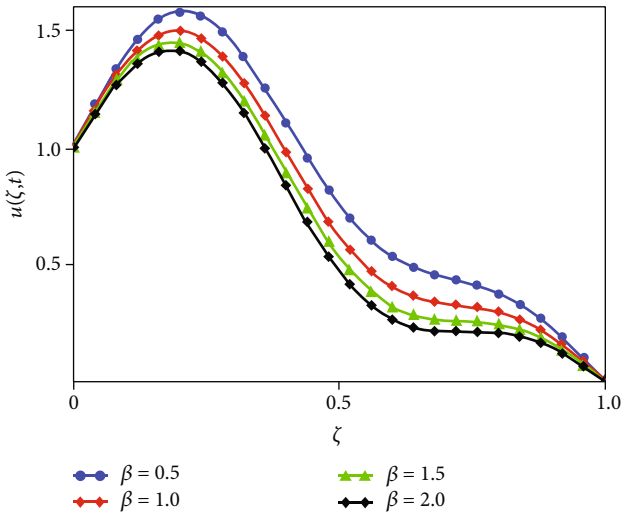

Figure 3: Impact of different values of β on velocity profile.

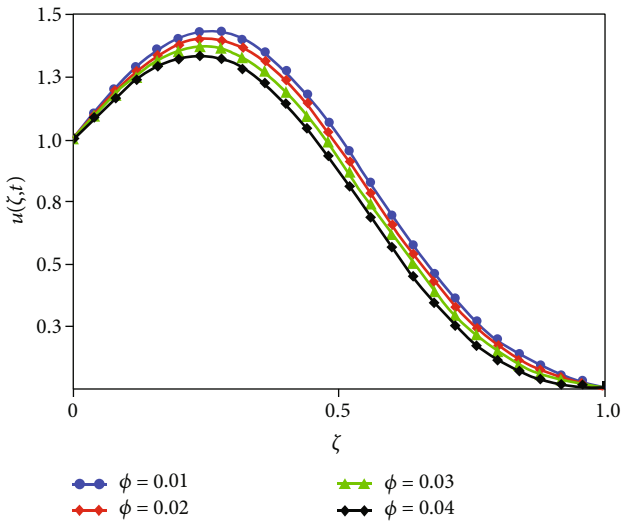

Figure 4: Impact of different values of ϕ on velocity profile.

Equations (19) and (20) may be written using the Caputo fractional derivative.

$$\frac{\partial T(\zeta,t)}{\partial t} = \frac{b_6}{b_5 \mathrm{Pr}} {}^{C}D_t^{1-\alpha} \frac{\partial^2 T(\zeta,t)}{\partial \zeta^2}, \tag{24}$$

$$\mathrm{Sc}\frac{\partial C(\zeta,t)}{\partial t} = \frac{1}{b_7} {}^{C}D_t^{1-\alpha} \left(\frac{\partial^2 C(\zeta,t)}{\partial \zeta^2}\right). \tag{25}$$

In order to derive the simplified form of Equations (24) and (25), we consider the time-fractional integral operator:

$$v_t^{\alpha}(K_1(\zeta,t)) = \left(\xi_{1-\alpha} {}^{*} K_1\right)(t) = \frac{1}{\Gamma(\alpha)} \int_0^t (t-s)^{\alpha-1} K_1(\zeta,s) ds. \tag{26}$$

The inverse operator of the fractional derivative ${}^{C}D_t^{\alpha}$ described in Equation (26) is Equation (21). Equations (24) and (25) may be expressed using the properties described in [39] as follows:

$${}^{C}D_t^{\alpha} T(\zeta,t) = \frac{b_6}{b_5 \mathrm{Pr}} \left(\frac{\partial^2 T(\zeta,t)}{\partial \zeta^2}\right), \tag{27}$$

$${}^{C}D_t^{\alpha} C(\zeta,t) = \frac{1}{b_7 \mathrm{Sc}} \left(\frac{\partial^2 C(\zeta,t)}{\partial \zeta^2}\right). \tag{28}$$

3. Solution of the Problem

3.1. Solution of Energy Field. When we apply the LT to Equation (27), we obtain

$$\mathrm{Pr} s^{\alpha} \bar{T}(\zeta,s) = \frac{b_6}{b_5} \left(\frac{d^2 \bar{T}(\zeta,s)}{d\zeta^2}\right), \tag{29}$$

and the transformed ICs and BCs are given by

$$\left.\begin{aligned} &\bar{u}(\zeta,t) = \bar{T}(\zeta,t) = ,\bar{C}(\zeta,0) = 0, t = 0, \\ &\bar{u}(\zeta,s) = \bar{T}(\zeta,s) = \bar{C}(\zeta,s) = \frac{1}{s}, \frac{\partial^2 \bar{u}(\zeta,s)}{\partial \zeta^2} = 0, \zeta = 0, \\ &\bar{T}(\zeta,s) = \bar{C}(\zeta,s) = \bar{u}(\zeta,s) = \frac{\partial^2 \bar{u}(\zeta,s)}{\partial \zeta^2} = 0, \zeta = 1. \end{aligned}\right\} \tag{30}$$

Now, using the conditions in Equation (30), we apply the FSFT to Equation (29), and we get

$$\bar{T}(k,s) = \frac{k\pi b_6}{b_5 \mathrm{Pr}} \left(\frac{1}{s(s^{\alpha}+L)}\right), \tag{31}$$

where $L = (k\pi)^2 (b_6/\mathrm{Pr} b_5)$.

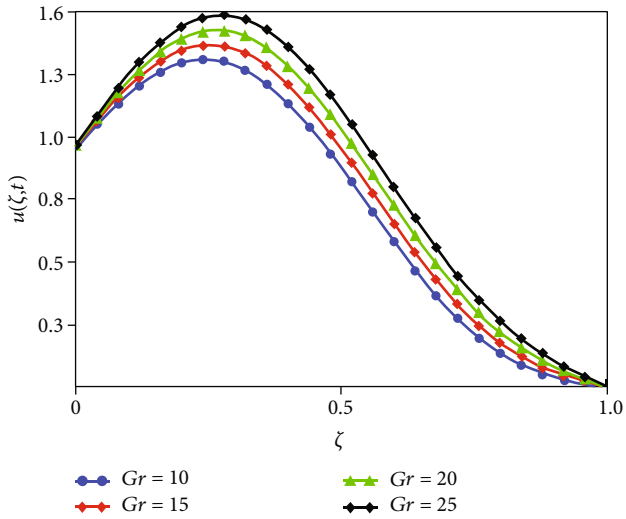

Figure 5: Impact of different values of Gr on velocity profile.

When inverse transformations are used, Equation (31) looks like this:

$$T(\zeta, t) = (1-\zeta) - 2\sum_{k=1}^{\infty} \frac{1}{k\pi} \cdot E_{\alpha}\left(\frac{-(k\pi)^2 t^{\alpha}}{\mathrm{Pr}} \frac{b_6}{b_5}\right) \sin(k\pi\zeta). \tag{32}$$

3.2. Solution of Concentration Field. Applying the LT to Equation (28), we get the following:

$$s^{\alpha}\bar{C}(\zeta, s) = \frac{1}{\mathrm{Sc}b_7}\left(\frac{d^2\bar{C}(\zeta, s)}{d\zeta^2}\right). \tag{33}$$

Now, using the conditions in Equation (30), we apply the FSFT to Equation (33), and we get

$$\bar{C}(k, s) = \frac{k\pi}{b_7\mathrm{Sc}}\left(\frac{1}{s\left(s^{\alpha} + L'\right)}\right), \tag{34}$$

where $L' = (k\pi)^2/\mathrm{Sc}$.

When inverse LT and FSFT are used, Equation (31) looks like this:

$$C(\zeta, t) = (1-\zeta) - 2\sum_{k=1}^{\infty} \frac{1}{k\pi} \cdot E_{\alpha}\left(\frac{-(k\pi)^2 t^{\alpha}}{b_7\mathrm{Sc}}\right) \sin(k\pi\zeta), \tag{35}$$

when the Mittag-Leffler function $E_{\alpha}(-\alpha t^{\alpha}) = \sum_{k=0}^{\infty}(-\alpha t)^k / \Gamma(\alpha k + 1)$ is used.

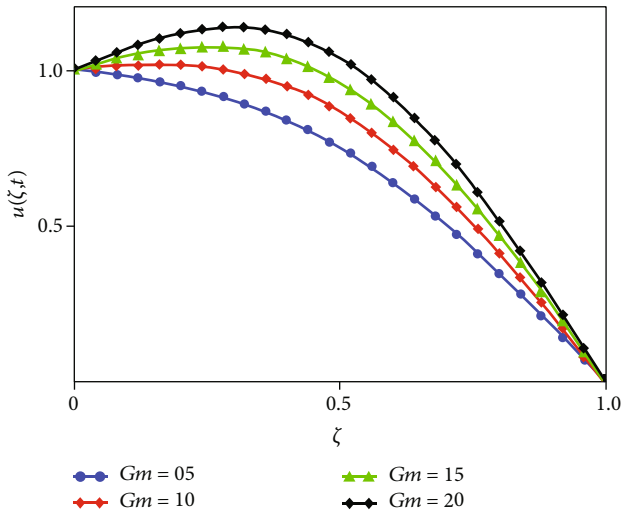

Figure 6: Impact of different values of Gm on velocity profile.

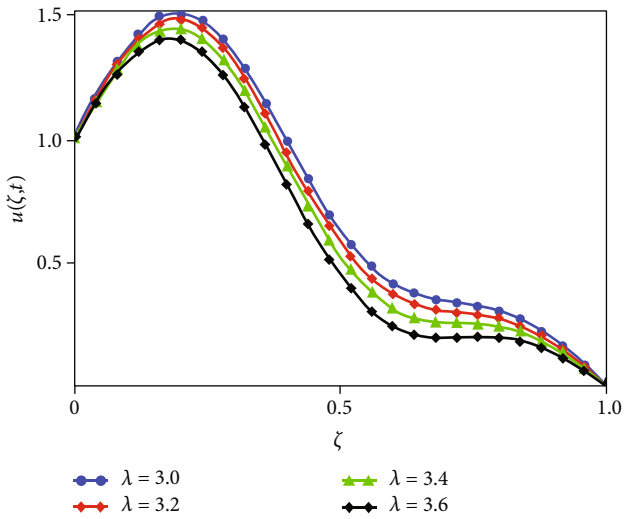

Figure 7: Impact of different values of λ on velocity profile.

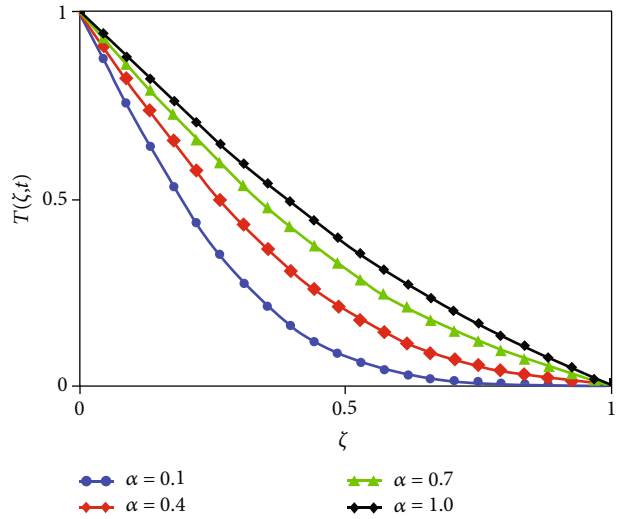

Figure 8: Impact of α on temperature distribution.

3.3. Solution of Momentum Equation. LT applied to Equation (12) allows us to write

$$\bar{u}(\zeta,s)=\frac{b_2}{b_1}\left(1+\frac{1}{\beta}\right)\frac{d^2\bar{u}(\zeta,s)}{d\zeta^2}-\frac{\lambda}{b_1}\frac{d^4\bar{u}(\zeta,s)}{d\zeta^4}+\frac{b_4}{b_1}\mathrm{Gm}\cos(\gamma)\bar{C}(\zeta,s)+\frac{1}{b_1}b_3\mathrm{Gr}\cos(\gamma)\bar{T}(\zeta,s). \tag{36}$$

Using Equation (36), the finite Fourier sine transform, and the substitution of Equations (31) and (34), we obtain

$$\bar{u}(k,s)=\frac{R_1}{R_2 s}+\frac{R_1}{R_2(s+R_2)}+\frac{b_6}{b_5}\frac{Grk\pi}{\mathrm{Pr}R_2}\frac{b_3}{b_1}\cos(\gamma)\left(\frac{1}{s(s^\alpha+L)}-\frac{1}{(s+R_2)(s^\alpha+L)}\right)+\frac{\mathrm{Gm}k\pi}{b_7\mathrm{Sc}R_2}\frac{b_4}{b_1}\cos(\gamma)\left(\frac{1}{s\left(s^\alpha+L'\right)}-\frac{1}{(s+R_2)\left(s^\alpha+L'\right)}\right). \tag{37}$$

Applying the inverse LT, we get the following expression for Equation (37).

$$\bar{u}(k,t)=\frac{R_1}{R_2}\left(1+e^{-R_2t}\right)+\frac{\mathrm{Gr}}{k\pi}\frac{b_3}{b_1}\cos(\gamma)\left(1-E_\alpha\left(\frac{b_6}{b_5}\frac{-(k\pi)^2}{\mathrm{Pr}}t^\alpha\right)\right)+\frac{\mathrm{Gm}}{k\pi}\frac{b_4}{b_1}\cos(\gamma)\left(1-E_\alpha\left(\frac{-(k\pi)^2}{b_7\mathrm{Sc}}t^\alpha\right)\right)-\frac{b_6}{b_5}\frac{\mathrm{Gr}k\pi}{\mathrm{Pr}R_2}\frac{b_3}{b_1}\cos(\alpha)\int_0^\tau t^{\alpha-1}E_{\alpha,\alpha}(-Lt^\alpha)*e^{-R_2(t-\tau)}d\tau-\frac{\mathrm{Gm}k\pi}{\mathrm{Sc}b_7R_2}\frac{b_4}{b_1}\cos(\alpha)\int_0^\tau t^{\alpha-1}E_{\alpha,\alpha}\left(-L't^\alpha\right)*e^{-R_2(t-\tau)}d\tau. \tag{38}$$

The final accurate solution to Equation (36) is obtained by transforming Equation (36) using inverse FSFT.

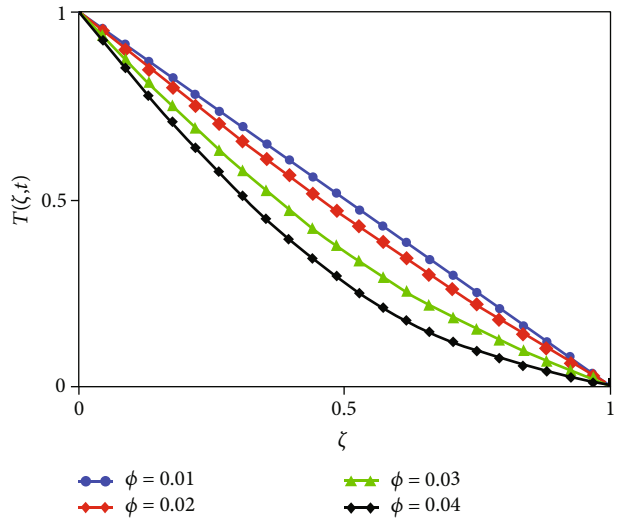

Figure 9: Impact of ϕ on temperature distribution.

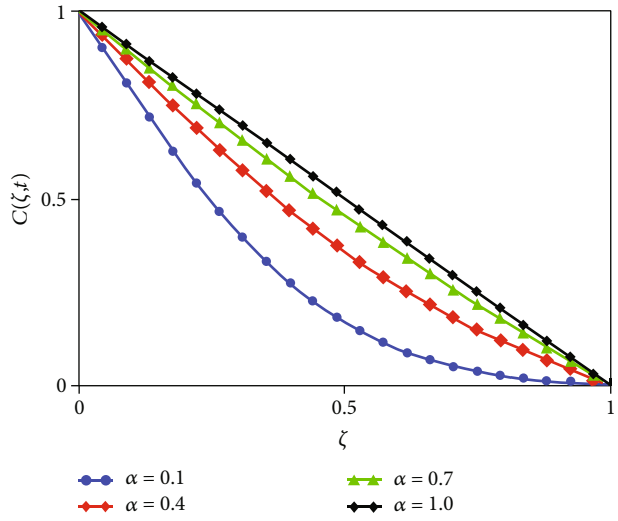

Figure 10: Impact of α on concentration distribution.

$$u(\zeta,t)=\left\{\begin{array}{l}(1-\zeta)+2\sum_{k=1}^{\infty}\frac{1}{k\pi}\exp(-k\pi R_2t)\sin(k\pi\zeta)+2\mathrm{Gr}\frac{b_3}{b_1}\cos(\gamma)\sum_{k=1}^{\infty}\frac{1}{k\pi}\left(1-E_\alpha\left(\frac{b_6}{b_5}\frac{-(k\pi)^2}{\mathrm{Pr}}t^\alpha\right)\right)\sin(k\pi\zeta)\\ +2\mathrm{Gm}\frac{b_4}{b_1}\cos(\gamma)\sum_{k=1}^{\infty}\frac{1}{k\pi}\left(1-E_\alpha\left(\frac{-(k\pi)^2}{b_7\mathrm{Sc}}t^\alpha\right)\right)\sin(k\pi\zeta)-2\frac{b_6}{b_5}\frac{\mathrm{Gr}}{\mathrm{Pr}}\frac{b_3}{b_1}\cos(\gamma)\sum_{k=1}^{\infty}\frac{k\pi}{R_2}\sin(k\pi\zeta)\\ \int_0^\tau t^{\alpha-1}E_{\alpha,\alpha}(-Lt^\alpha)\times e^{-R_2(t-\tau)}d\tau-2\frac{\mathrm{Gm}}{b_7\mathrm{Sc}}\frac{b_4}{b_1}\cos(\gamma)\sum_{k=1}^{\infty}\frac{k\pi}{R_2}\sin(k\pi\zeta)\int_0^\tau t^{\alpha-1}E_{\alpha,\alpha}\left(-L't^\alpha\right)\times e^{-R_2(t-\tau)}d\tau\end{array}\right\}, \tag{39}$$

where $R=(b_2/b_1)(1+(1/\beta)),R_1=R(k\pi)+(\lambda/b_1)(k\pi)^3$, and $R_2=k\pi R_1$.

3.4. Skin Friction and Nusselt Number. The comparative from Ahmad et al. [39] obtains skin friction terms from Equation (39) and Nusselt number expressions from Equation (32).

$$\mathrm{Cf} = \frac{1}{(1-\phi)^{2.5}}\left(1+\frac{1}{\beta}\right)\frac{\partial u(\zeta,t)}{\partial \zeta}\bigg|_{\zeta=0} - \lambda\frac{\partial^3 u(\zeta,t)}{\partial \zeta^3}\bigg|_{\zeta=0},$$
$$\mathrm{Nu} = -b_6\frac{\partial T(\zeta,t)}{\partial \zeta}\bigg|_{\zeta=0}. \tag{40}$$

4. Result and Discussion

An investigation of the unsteady, unidirectional, and incompressible flow of couple stress SA-based Casson nanofluid through inclined microchannel is worked out in this article. A fractional model is developed by using the laws of Fourier and Fick, respectively. By combining the Laplace and Fourier finite sine transforms, it is possible to find closed-form solutions. After being calculated and put into a table, the skin friction, Sherwood number, and Nusselt number of the boundary layer flow are each given as a number. Figures 2–12 show how the distributions of speed, temperature, and concentration change when different embedded parameters are changed.

Figures 2, 8, and 10 demonstrate how the fractional parameter α impacts the profile of fluid velocity, the distribution of temperatures, and the distribution of concentrations. Different integral velocity profiles are created, which is different from the classical model. The easiest way to fit these many integral profiles might be to use real data or results from experiments.

Figure 3 shows what happens to the speed profile when the Casson parameter β is changed. When the value of the Casson parameter β rises, the flow decelerates, as shown by the graphs. The science behind this is that when the value of β is raised, the viscous forces that provide resistance and slow the flow are also raised.

The effects of volume friction ϕ on velocity profile, temperature distribution, and concentration distribution are depicted in Figures 4, 9, and 11. As a result of sedimentation, the range is between 0 and 0.04 when it reaches 0.08 when it is measured. A rise in the nanoparticle volume friction percentage will, in either scenario, result in a lower temperature, as well as a change in the concentration distribution and the velocity profile.

Figures 5 and 6 show how Gr and Gm influence the velocity of the SA-based Casson nanofluid under CS. These pictures show that a function of these values that rises implies that the velocity goes up. Because they are going up, the buoyancy forces are going up, which causes the viscosity of the fluid to move down, which makes the fluid move faster. There is evidence that this statement is true.

The velocity profile flattens out when the couple stress parameter λ drops, as seen in Figure 7, which shows how λ affects velocity. Physics-wise, this behavior happens because increasing λ also increases the viscosity, which slows the Casson nanofluid based on SA.

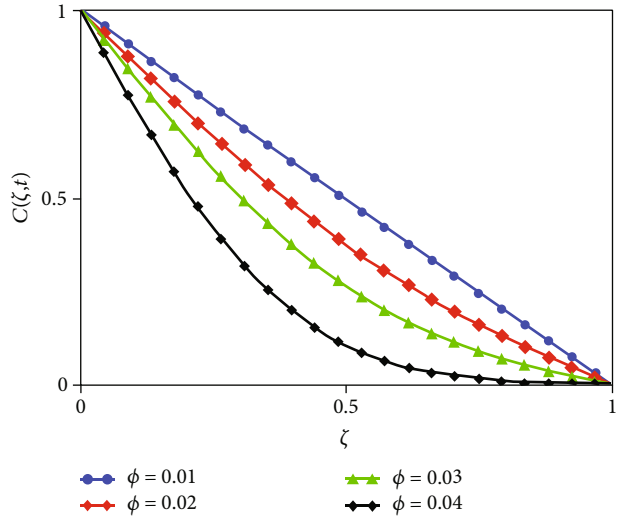

Figure 11: Impact of ϕ on concentration distribution.

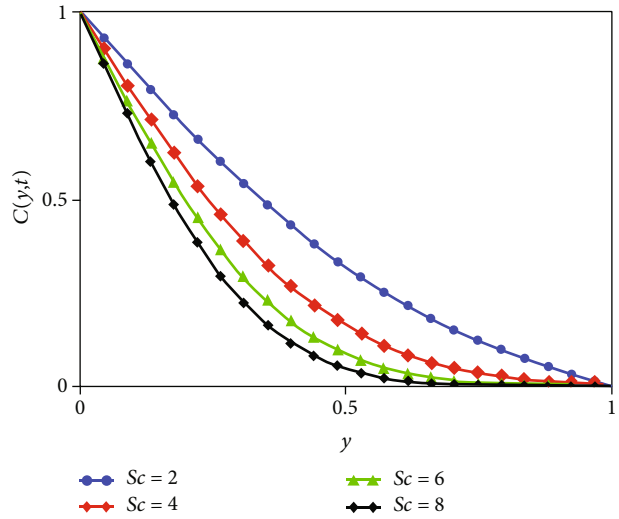

Figure 12: Impact of Sc on concentration distribution.

Table 1: Thermophysical properties.

Material	Base fluids	Nanoparticles			
	SA	Al_2O_3	Cu	TiO_2	Ag
$\rho(\mathrm{kg/m^3})$	989	3970	8933	4250	10500
$c_p(\mathrm{J/kgK})$	4175	765	385	686.2	235
$K(\mathrm{W/mK})$	0.613	40	401	8.9528	429
$\beta \times 10^{-5}(\mathrm{K^{-1}})$	0.99	0.85	1.67	0.9	1.89

The concentration is shown in Figure 12 for various Schmidt number Sc values. As the Schmidt number rises, the concentration boundary layer thickness falls. The Schmidt number decreased both the consecration and the

Table 2: The effect of different parameters onCf.

t	α	β	λ	ϕ	Gm	Gr	Cf
0.9	0.5	2	2	0.01	5	2	**1.06033**
0.9	**0.6**	2	2	0.01	5	2	**1.00032**
0.9	0.5	**3**	2	0.01	5	2	**4.00632**
0.9	0.5	2	**4**	0.01	5	2	**5.23687**
0.9	0.5	2	2	**0.03**	5	2	**1.71032**
0.9	0.5	2	2	0.01	**10**	2	**0.23124**
0.9	0.5	2	2	0.01	5	**3**	**0.91119**

Table 3: The effect of different parameters on Nu.

t	α	ϕ	Nu
1	0.5	0.01	2.32203
1.5	0.5	0.01	2.92772
1	0.6	0.01	2.00024
1	0.5	0.03	3.94575

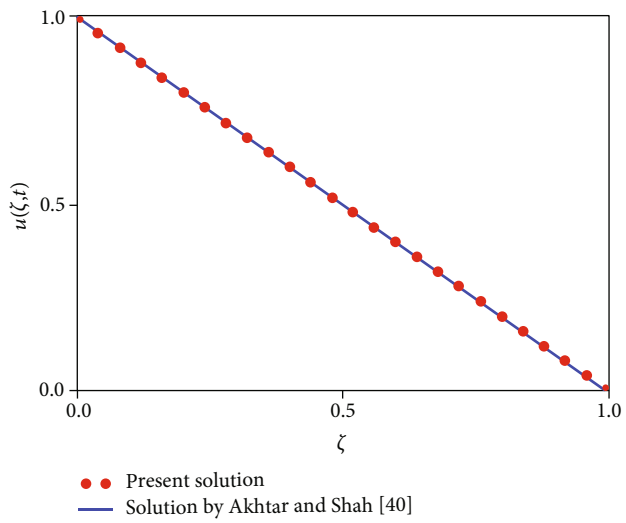

Figure 13: Comparison of the current solution with Akhtar and Shah [40].

velocity profile since it measures the proportion of viscous forces to mass diffusivity. Physically, the velocity of the SA-based Casson nanofluid decreases as viscous forces rise.

Table 1 displays the thermophysical characteristics of nanoparticles for your review. Table 2 displays the variation in skin friction caused by different parameter values. Skin friction is significant in several engineering areas, especially civil engineering. The viscous forces and, consequently, the surface friction increase as β raises. Skin friction is decreased by raising Gr and Gm. By raising Gr and Gm, the buoyancy forces rise, the viscosity drops, and the surface friction goes down as a result. Table 2 clearly illustrates how skin friction reduces as volume friction ϕ increases.

The Nusselt number is shown in Table 3. An increase in momentum diffusivity leads to a decrease in the thickness of the thermal boundary layer, which in turn decreases the Nusselt number since the Prandtl number Pr measures the relationship between momentum and thermal diffusivity. By putting $\alpha = 1, M = 0, \mathrm{Gr} = \mathrm{Gm} = 0, t = 1, \beta \longrightarrow \infty$, and $\phi = 0$, our solution is reduced to the solution of Akhtar and Shah [40], which is presented in Figure 13, which validates our solution.

5. Conclusion

This article describes how the classical model is now turned into a time-fractional model utilizing Fick's and Fourier's equations in line with Caputo's definition. Laplace and Fourier integral transforms are used to get accurate solutions. Visual illustrations and physical descriptions are used to show how different embedded elements affect the distributions of velocity, temperature, and concentration. The present work's main conclusions are as follows:

(1) Using Fick's and Fourier's laws, the time derivative is adapted into a time-fractional model

(2) The fractional models offer a wider range of answers since they are more realistic. Considering the relevant data, these solutions could be the best

(3) In accordance with the concept of skin friction, the impact of different variables on skin friction is completely different from the impact of velocity

(4) By increasing the volume friction, as a result, the temperature profile, concentration profile, and velocity profile decrease

Nomenclature

$\vec{V}$: Velocity vector
k_{nf}: Thermal conductivity of the nanofluid
T_d: Embedded temperature
C_d: Embedded concentration
$\vec{b}_1$: Body force vector
ρ_{nf}: Density of nanofluid
g: Gravitational acceleration
$(\beta_T)_{\mathrm{nf}}$: Coefficient of thermal expansion of nanofluid
$(Cp)_{\mathrm{nf}}$: Heat capacitance of the nanofluid
$\vec{C}$: Concentration vector
$\vec{T}$: Temperature vector
p: Pressure
μ_{nf}: Dynamic viscosity of nanofluid
λ: Couple stress parameter
β: Casson fluid parameter
γ: Inclination angle
$\pi = e_{ab}$: Factor of the deformation rate
μ_n: Plastic dynamic viscosity
P_λ: Yield stress of fluid
Nu: Nusselt number
Cf: Skin friction
Gr: Grashof number
Gm: Mass Grashof number

Pr: Prandtl number
Sc: Schmidt number
ϕ: Volume friction of nanofluid
$C(\zeta, t)$: Concentration
$T(\zeta, t)$: Temperature
$V(\zeta, t)$: Velocity
d: Distance between parallel plates
D_{nf}: Thermal diffusivity of nanofluid.

Data Availability

All the data used is available in the manuscript.

Conflicts of Interest

The authors declare no competing interests.

Authors' Contributions

Dolat Khan was responsible for supervision, methodology, and draft writing; Musawa Yahya Almusawa was the project administrator and responsible for methodology; M. Ali Akbar was responsible for funding and draft writing; Waleed Hamali was responsible for the investigation, methodology, and draft writing.

References

[1] S. K. Das, N. Putra, P. Thiesen, and W. Roetzel, "Temperature dependence of thermal conductivity enhancement for nanofluids," *Journal of Heat Transfer*, vol. 125, no. 4, pp. 567–574, 2003.

[2] S. U. Choi and J. A. Eastman, "Enhancing thermal conductivity of fluids with nanoparticles," (No. ANL/MSD/CP-84938; CONF-951135-29). Argonne National Lab.(ANL), Argonne, IL (United States), 1995.

[3] V. Karthik, S. Sahoo, S. K. Pabi, and S. Ghosh, "On the phononic and electronic contribution to the enhanced thermal conductivity of water-based silver nanofluids," *International Journal of Thermal Sciences*, vol. 64, pp. 53–61, 2013.

[4] J. A. Eastman, S. U. S. Choi, S. Li, W. Yu, and L. J. Thompson, "Anomalously increased effective thermal conductivities of ethylene glycol-based nanofluids containing copper nanoparticles," *Applied Physics Letters*, vol. 78, no. 6, pp. 718–720, 2001.

[5] Q. Li, Y. M. Xuan, J. Jiang, and J. W. Xu, "Experimental investigation on flow and convective heat transfer feature of a nanofluid for aerospace thermal management," *Yuhang Xuebao/Journal of Astronautics(China)*, vol. 26, no. 4, pp. 391–394, 2005.

[6] S. Z. Heris, S. G. Etemad, and M. N. Esfahany, "Experimental investigation of oxide nanofluids laminar flow convective heat transfer," *International Communications in Heat and Mass Transfer*, vol. 33, no. 4, pp. 529–535, 2006.

[7] S. K. Das, S. U. Choi, W. Yu, and T. Pradeep, *Nanofluids: Science and Technology*, John Wiley & Sons, 2007.

[8] D. J. Faulkner, D. R. Rector, J. J. Davidson, and R. Shekarriz, "Enhanced heat transfer through the use of nanofluids in forced convection," in *ASME International Mechanical Engineering Congress and Exposition (Vol. 4711, pp. 219-224)*, Anaheim, California, USA, 2004.

[9] W. Y. Lai, B. Duculescu, P. E. Phelan, and R. S. Prasher, "Convective heat transfer with nanofluids in a single 1.02-mm tube," in *ASME International Mechanical Engineering Congress and Exposition (Vol. 47861, pp. 337-342)*, Chicago, Illinois, USA, 2006.

[10] Y. Xuan and Q. Li, "Investigation on convective heat transfer and flow features of nanofluids," *Journal of Heat Transfer*, vol. 125, no. 1, pp. 151–155, 2003.

[11] A. Khan, D. Khan, I. Khan, F. Ali, and M. Imran, "MHD flow of sodium alginate-based Casson type nanofluid passing through a porous medium with Newtonian heating," *Scientific Reports*, vol. 8, no. 1, pp. 1–12, 2018.

[12] S. Oka, "An approach to α unified theory of the flow behavior of time-independent non-Newtonian suspensions," *Japanese Journal of Applied Physics*, vol. 10, no. 3, p. 287, 1971.

[13] K. Ahmad, Z. Hanouf, and A. Ishak, "MHD Casson nanofluid flow past a wedge with Newtonian heating," *The European Physical Journal Plus*, vol. 132, no. 2, pp. 1–11, 2017.

[14] D. Khan, A. Khan, I. Khan, F. Ali, and I. Tlili, "Effects of relative magnetic field, chemical reaction, heat generation and Newtonian heating on convection flow of Casson fluid over a moving vertical plate embedded in a porous medium," *Scientific Reports*, vol. 9, no. 1, pp. 1–18, 2019.

[15] J. Mackolil and B. Mahanthesh, "Exact and statistical computations of radiated flow of nano and Casson fluids under heat and mass flux conditions," *Journal of Computational Design and Engineering*, vol. 6, no. 4, pp. 593–605, 2019.

[16] B. Mahanthesh, "Statistical and exact analysis of MHD flow due to hybrid nanoparticles suspended in $C_2H_6O_2$-H_2O hybrid base fluid," in *Mathematical Methods in Engineering and Applied Sciences*, pp. 185–228, CRC Press, 2020.

[17] J. Mackolil and B. Mahanthesh, "Time-dependent nonlinear convective flow and radiative heat transfer of Cu-Al_2O_3-H_2O hybrid nanoliquid with polar particles suspension: a statistical and exact analysis," *BioNanoScience*, vol. 9, no. 4, pp. 937–951, 2019.

[18] B. Mahanthesh, T. S. Ashlin, B. J. Gireesha, S. A. Shehzad, and M. N. Bashir, "Time-dependent flow due to noncoaxial rotation of an infinite vertical surface subjected to an exponential space-dependent heat source: an exact analysis," *Research*, vol. 48, no. 7, pp. 3162–3185, 2019.

[19] P. V. Satya Narayana, N. Tarakaramu, G. Sarojamma, and I. L. Animasaun, "Numerical simulation of nonlinear thermal radiation on the 3D flow of a couple stress Casson nanofluid due to a stretching sheet," *Journal of Thermal Science and Engineering Applications*, vol. 13, no. 2, 2021.

[20] T. D. Dass, S. R. Gunakala, and D. M. Comissiong, "Combined effect of variable-viscosity and surface roughness on the squeeze film characteristics of infinitely wide rectangular plate with couple stress fluid, velocity-slip and ferrofluid lubricant," *Materials Today: Proceedings*, vol. 56, pp. 1717–1725, 2022.

[21] V. K. Stokes, *Theories of Fluids with Microstructure: An Introduction*, Springer Science & Business Media, 2012.

[22] B. Mahanthesh, B. J. Gireesha, N. S. Shashikumar, T. Hayat, and A. Alsaedi, "Marangoni convection in Casson liquid flow due to an infinite disk with exponential space dependent heat source and cross-diffusion effects," *Results in Physics*, vol. 9, pp. 78–85, 2018.

[23] S. O. Adesanya and O. D. Makinde, "Effects of couple stresses on entropy generation rate in a porous channel with convective heating," *Computational and Applied Mathematics*, vol. 34, no. 1, pp. 293–307, 2015.

[24] E. A. Ashmawy, "Unsteady Couette flow of a micropolar fluid with slip," *Meccanica*, vol. 47, no. 1, pp. 85–94, 2012.

[25] D. Khan, G. Ali, P. Kumam, M. Y. Almusawa, and A. M. Galal, "Time fractional model of free convection flow and dusty two-phase couple stress fluid along vertical plates," *ZAMM-Journal of Applied Mathematics and Mechanics/Zeitschrift für Angewandte Mathematik und Mechanik*, article e202200369, 2016.

[26] F. Ali, Z. Ahmad, M. Arif, I. Khan, and K. S. Nisar, "A time fractional model of generalized Couette flow of couple stress nanofluid with heat and mass transfer: applications in engine oil," *IEEE Access*, vol. 8, pp. 146944–146966, 2020.

[27] R. Gorenflo and F. Mainardi, "Fractional calculus," in *Fractals and Fractional Calculus in Continuum Mechanics*, pp. 223–276, Springer, Vienna, 1997.

[28] B. Ross, "The development of fractional calculus 1695-1900," *Historia Mathematica*, vol. 4, no. 1, pp. 75–89, 1977.

[29] T. F. Nonnenmacher and R. Metzler, "On the Riemann-Liouville fractional calculus and some recent applications," *Fractals*, vol. 3, no. 3, pp. 557–566, 1995.

[30] S. Jiang, J. Zhang, Q. Zhang, and Z. Zhang, "Fast evaluation of the Caputo fractional derivative and its applications to fractional diffusion equations," *Communications in Computational Physics*, vol. 21, no. 3, pp. 650–678, 2017.

[31] J. M. Cruz-Duarte, J. Rosales-Garcia, C. R. Correa-Cely, A. Garcia-Perez, and J. G. Avina-Cervantes, "A closed form expression for the Gaussian-based Caputo-Fabrizio fractional derivative for signal processing applications," *Communications in Nonlinear Science and Numerical Simulation*, vol. 61, pp. 138–148, 2018.

[32] Y. Yang, W. Xu, W. Jia, and Q. Han, "Stationary response of nonlinear system with Caputo-type fractional derivative damping under Gaussian white noise excitation," *Nonlinear Dynamics*, vol. 79, no. 1, pp. 139–146, 2015.

[33] M. Caputo, "Linear models of dissipation whose Q is almost frequency independent—II," *Geophysical Journal International*, vol. 13, no. 5, pp. 529–539, 1967.

[34] E. F. D. Goufo, "Application of the Caputo-Fabrizio fractional derivative without singular kernel to Korteweg-de Vries-Burgers equation," *Mathematical Modelling and Analysis*, vol. 21, no. 2, pp. 188–198, 2016.

[35] M. Caputo and M. Fabrizio, "A new definition of fractional derivative without singular kernel," *Progress in Fractional Differentiation & Applications*, vol. 1, no. 2, pp. 1–13, 2015.

[36] P. Kumam and W. Watthayu, "A novel comparative case study of entropy generation for natural convection flow of proportional-Caputo hybrid and Atangana baleanu fractional derivative," *Scientific Reports*, vol. 11, no. 1, pp. 1–11, 2021.

[37] D. Khan, A. ur Rahman, P. Kumam, W. Watthayu, K. Sitthithakerngkiet, and A. M. Galal, "Thermal analysis of different shape nanoparticles on hyperthermia therapy on breast cancer in a porous medium: a fractional model," *Heliyon*, vol. 8, no. 8, article e10170, 2022.

[38] S. Akhtar, "Flows between two parallel plates of couple stress fluids with time-fractional Caputo and Caputo-Fabrizio derivatives," *The European Physical Journal Plus*, vol. 131, no. 11, pp. 1–13, 2016.

[39] S. Ahmad, S. U. Haq, F. Ali, I. Khan, and K. S. Nisar, "Time fractional analysis of channel flow of couple stress Casson fluid using Fick's and Fourier's laws," *Scientific Reports*, vol. 12, no. 1, pp. 1–16, 2022.

[40] S. Akhtar and N. A. Shah, "Exact solutions for some unsteady flows of a couple stress fluid between parallel plates," *Ain Shams Engineering Journal*, vol. 9, no. 4, pp. 985–992, 2018.